

$Li_{10}Bi$: A lithium-rich electride with coexisting superconductivity and solid-state lithium-ion conductivity

Jingkun Yu(于镜坤), Xue Yong(雍雪), and Siyu Lu(卢思宇)
Citation: Chin. Phys. B, 2026, 35 (**5**): 057402. DOI: 10.1088/1674-1056/ae306d
http://cpb.iphy.ac.cn; http://iopscience.iop.org/cpb

What follows is a list of articles you may be interested in

Manipulating the electronic structure and superconductivity of Li_2B_3C by biaxial strain

Yuhao Gu(顾雨豪), Yihao Wang(王奕淏), and Shuxian Hu(胡淑贤)
Chin. Phys. B, 2026, 35 (**4**): 047401. DOI: 10.1088/1674-1056/ae5594

High-throughput discovery and electron-doping tuning of superconducting ternary lithium borides

Bohan Cao(曹博瀚), Xinwei Wang(王新伟), Yibo Sun(孙一博), Mengxin Yang(杨孟鑫), Defang Duan(段德芳), Fubo Tian(田夫波), and Tian Cui(崔田)
Chin. Phys. B, 2026, 35 (**3**): 037401. DOI: 10.1088/1674-1056/ae27b1

Doping-dependent optical properties in YBCO superconducting films via $BaHfO_3$ nanocrystal addition

Shulun Han(韩淑伦), Yuanjie Ning(宁苑杰), Jing Chen(陈静), Yanqun Guo(郭艳群), Zicong Yang(杨子聪), Ping Zhu(朱萍), Zhigang Zeng(曾志刚), Chuanbing Cai(蔡传兵), Xinmao Yin(尹鑫茂), and Lijun Tian(田立君)
Chin. Phys. B, 2026, 35 (**2**): 027404. DOI: 10.1088/1674-1056/adee87

Exotic superconductivity in new topological kagome metal $CsTi_3Bi_5$

Jiali Liu(刘家利), Zhen Zhao(赵振), Hongqin Xiao(肖洪钦), Yuhang Zhang(张宇航), Zouyouwei Lu(鲁邹有为), Jihu Lu(卢佶虎), Feng Wu(吴凤), Chengjie Xu(徐诚杰), Hua Zhang(张华), Hui Chen(陈辉), Haitao Yang(杨海涛), Ziyi Liu(刘子儀), Xiaoli Dong(董晓莉), and Hongjun Gao(高鸿钧)
Chin. Phys. B, 2026, 35 (**2**): 027403. DOI: 10.1088/1674-1056/ae2c6d

Pressure-stabilized Li_2K electride with superconducting behavior

Xiao-Zhen Yan(颜小珍), Quan-Xian Wu(邬泉县), Lei-Lei Zhang(张雷雷), and Yang-Mei Chen(陈杨梅)
Chin. Phys. B, 2025, 34 (**9**): 097405. DOI: 10.1088/1674-1056/add009

SPECIAL TOPIC — John Tse: Pioneer in high-pressure materials science

$Li_{10}Bi$: A lithium-rich electride with coexisting superconductivity and solid-state lithium-ion conductivity

Jingkun Yu(于镜坤)[1], Xue Yong(雍雪)[2,†], and Siyu Lu(卢思宇)[1,‡]

[1] *College of Chemistry and Pingyuan Laboratory, Zhengzhou University, Zhengzhou* 450001, *China*
[2] *Department of Electrical Engineering and Electronics, University of Liverpool, Liverpool, United Kingdom*

(Received 14 November 2025; revised manuscript received 20 December 2025; accepted manuscript online 23 December 2025)

Electrides, characterized by interstitial quasi-atoms (ISQs) where electrons occupy lattice voids instead of atomic orbitals, provide a unique platform for discovering novel superconductors and mixed-conduction materials. Here, using crystal structure prediction combined with first-principles calculations, we systematically explore lithium-rich Li–Bi compounds under high pressure. Several new Li-rich stoichiometries, LiBi, $Li_{11}Bi_2$, Li_9Bi, and $Li_{10}Bi$, are identified as thermodynamically stable. Among them, the $C2/m$ phase of $Li_{10}Bi$ features one-dimensional ISQ networks, exhibiting both metallic and electride characteristics. Electron–phonon coupling analysis reveals a dome-shaped evolution of superconducting transition temperature (T_c), reaching a maximum value of 9.9 K at 35 GPa, where the superconductivity is primarily driven by strong Li-derived phonon modes. *Ab initio* molecular dynamics simulations further reveal a temperature-induced superionic transition above 700 K, where Li^+ ions diffuse freely while Bi atoms remain fixed within the lattice. This coexistence of superconductivity and superionicity within a single crystalline framework highlights $Li_{10}Bi$ as a prototype dual-functional electride, bridging the gap between quantum superconductors and solid-state lithium-ion conductors. These findings open a new route for designing multifunctional materials that integrate electronic and ionic transport for next-generation energy and quantum applications.

Keywords: high pressure, electrides, structural search, superconductivity

PACS: 74.25.–q, 62.50.–p, 61.50.Ks

DOI: 10.1088/1674-1056/ae306d **CSTR:** 32038.14.CPB.ae306d

1. Introduction

Superconductors and solid-state electrolytes represent two extreme regimes of charge, the former mediated by Cooper-paired electrons with zero resistance, and the latter by highly mobile ions within a rigid lattice.[1–5] Bridging these two phenomena in a single crystalline material has long been of fundamental and technological interest, particularly for quantum devices and next-generation energy systems.[6,7]

Electrides, a unique class of quantum materials characterized by interstitial quasi-atoms (ISQs), offer a promising platform for realizing such dual behavior.[8–12] In these systems, a fraction of electrons occupies interstitial lattice voids rather than atomic orbitals, acting as anionic charge carriers.[13] The spatial confinement and connectivity of these interstitial electrons profoundly influence electron–phonon coupling (EPC), enabling unconventional superconductivity with high superconducting transition temperature (T_c).[14] Several high-pressure electrides such as Li_6P and Li_8Au have demonstrated T_c values up to 39.3 K and 73 K at several hundred gigapascals, illustrating the potential of ISQ-driven superconducting approaches.[15,16]

Lithium, as the lightest metal, plays a central role in both superconductivity and ion conduction: its low atomic mass promotes high phonon frequencies and fast ion mobility, and its electron affinity allows it to donate an electron to form ISQs.[17–21] Bismuth, conversely, is a heavy semimetal with strong spin-orbit coupling, providing a contrasting electronic environment and structural rigidity.[22–25] The Li–Bi system, therefore, presents an ideal ground for exploring how light-element lattice dynamics and heavy-element electronic correlations cooperatively determine transport properties.[26]

Here, we perform a comprehensive theoretical search of Li–Bi compounds under pressure and identify several new Li-rich phases, including $Li_{10}Bi$, which exhibits both superionic and superconducting behavior. The $C2/m$ phase of $Li_{10}Bi$ stands out due to its distinctive one-dimensional interstitial electrons, metallicity, and pressure-induced superconductivity with T_c up to 9.9 K. Moreover, *ab initio* molecular dynamics (AIMD) simulations reveal that $Li_{10}Bi$ undergoes a superionic transition at elevated temperatures, in which Li^+ ions diffuse freely while Bi atoms remain fixed in a rigid lattice. This coexistence of superconducting and superionic states establishes $Li_{10}Bi$ as a prototype for multifunctional electride materials and opens a new direction for designing hybrid quantum-ionic

†Corresponding author. E-mail: yongx837@liverpool.ac.uk
‡Corresponding author. E-mail: sylu2013@zzu.edu.cn

© 2026 Chinese Physical Society and IOP Publishing Ltd. All rights, including for text and data mining, AI training, and similar technologies, are reserved.

solids relevant to superconducting and solid-state battery technologies.

2. Computational methods

We have performed a structural search for possible compounds in the binary Li–Bi system (Li_xBi_y, $x = 1$–12, $y = 1$–2) using the particle swarm optimization algorithm of the CALYPSO software.[27,28] Structural relaxation and electronic calculations were performed using the Vienna *ab initio* simulation package (VASP), which is based on first-principles calculations in the framework of density functional theory (DFT).[29] The generalized gradient approximation (GGA) implemented by Perdew–Burke–Ernzerhof (PBE) was chosen as the exchange–correlation functional, with $1s^2 2s^1$ and $6s^2 6p^3$ valence electrons for Li and Bi atoms, respectively.[30] All calculations were performed self-consistently using the Monkhorst-Pack scheme with a k-point grid spacing of $2\pi \times 0.03$ Å^{-1} and a cutoff energy of 550 eV.[31] The structures were optimized until the maximum energy and force were less than 10^{-7} eV and 0.01 eV/Å, respectively. Using the previous wave function and electron number, a He atom was placed at the interstitial quasi-atom site, and the band structure and density of states of the interstitial quasi-atom were calculated. The thermodynamic stability of each stoichiometry with respect to elemental Li and Bi solids at each pressure can be evaluated by calculating the formation enthalpy as

$$\Delta H\left(\mathrm{Li}_x\mathrm{Bi}_y\right) = \frac{H\left(\mathrm{Li}_x\mathrm{Bi}_y\right) - xH\left(\mathrm{Li}\right) - yH(\mathrm{Bi})}{x+y}.$$

Here, $H(\mathrm{Li}_x\mathrm{Bi}_y)$, $H(\mathrm{Li})$, and $H(\mathrm{Bi})$ are the enthalpies of the studied stoichiometry, elemental Li, and Bi solids under the corresponding pressure, respectively. To identify and characterize the ISQs, we first used ELF analysis to locate the interstitial anionic electrons in $Li_{10}Bi$. The He-probe method was then applied by placing an inert He atom at each ELF-identified site, allowing the localized interstitial electron to be projected as a He-centered state. The He-projected density of states (PDOS) obtained from a non-self-consistent calculation directly represents the PDOS of the ISQs. Then, we used the phonopy package for dynamical stability calculations.[32] The superconducting properties were calculated using density functional perturbation theory based on the QUANTUM ESPRESSO software, in which the ultrasoft pseudopotential (USPP) was selected to describe the interaction between electrons and ions.[33] We sampled the k and q networks of the electron Brillouin zone integrals, with $12 \times 20 \times 24$ fine k-points and $3 \times 5 \times 6$ irreducible q-points, to assess the average contribution of the phonon modes. The Gaussian smearing method was used with a smearing parameter set to $\sigma = 0.02$ Ry. The T_c was calculated using the Allen–Dynes modified McMillan formula[34,35]

$$T_c = \frac{\omega_{\log}}{1.2}\exp\left[-\frac{1.04\,(1+\lambda)}{\lambda-\mu^*\,(1+0.62\lambda)}\right],$$

where μ^* is the Coulomb pseudopotential parameter. In our calculations, μ^* was set to a typical value of 0.1. AIMD simulations explore the atomic dynamical properties of $Li_{10}Bi$ at high pressures and high temperatures.[36,37] The NVT ensemble, applying a Nosé–Hoover thermostat combined with a supercell of 132 atoms, is employed with the Γ point for the Brillouin zone sampling.[38,39] Each simulation consists of 5000 time steps with a time step of 2 fs.

3. Results and discussion

3.1. New Li-rich electrides

Structure search for stable crystal structures and potential phase transitions in the Li_xBi_y ($x = 1$–12, $y = 1$–2) system was performed under high pressures ranging from 50 to 300 GPa. The simulations were carried out with unit cells containing up to four formula units (f.u.) to ensure sufficient configurational diversity. Our structural searches successfully reproduced previously reported Li–Bi compounds, including the *Fm*-3*m* phase of Li_3Bi and the *P*6/*mmm* phase of Li_5Bi, thereby validating the reliability of both the structure prediction methodology and the pseudopotentials used.[40]

Thermodynamic stability was assessed by calculating the enthalpy of formation of each compound relative to decomposition into the most stable elemental phases of Li and Bi at the corresponding pressure (Fig. 1(a)). Based on this convex hull, LiBi, Li_3Bi, Li_5Bi, $Li_{11}Bi_2$, Li_9Bi, and $Li_{10}Bi$ are the thermodynamically stable lithium-rich compounds. To compare their stability across different pressures, we also constructed a pressure-composition phase diagram, as shown in Fig. 1(b). Among them, LiBi and Li_3Bi remain thermodynamically stable from 50–300 GPa, with Li_3Bi (*Fm*-3*m*) being the most stable phase throughout. The *P*6/*mmm* phase of Li_5Bi is stable up to 112 GPa. Upon further compression, Li_5Bi undergoes two phase transitions: *P*-1 stable between 112 GPa and 281 GPa, and a *Cmcm* phase stable above 281 GPa. The *C*2/*m* phase of $Li_{11}Bi_2$ is stable between 178 GPa and 245 GPa. As the lithium content increases, the *P*-1 phase of Li_9Bi becomes stable above 185 GPa, while the *C*2/*m* phase of $Li_{10}Bi$ is stable in the range of 50–118 GPa. To assess finite-temperature effects, quasi-harmonic approximation (QHA) calculations were performed for *C*2/*m*-$Li_{10}Bi$, *P*6/*mmm*-Li_5Bi, and elemental Li at 50 GPa. The resulting Gibbs free energies show that *C*2/*m*-$Li_{10}Bi$ remains thermodynamically stable up to $\sim$ 3000 K, indicating that vibrational contributions do not alter the phase stability established at 0 K (Fig. S1). The predicted crystal structures for these compounds are illustrated in Fig. 2. With

the increase of Li content, the coordination environment of Bi atoms changes to super-coordinated, and all Li–Bi phases are densely assembled polyhedra. In general, all lithium-rich Bi compounds are composed of interconnected $BiLi_n$ polyhedra. Additionally, phonon dispersion calculations were performed for each structure under its respective stable pressure conditions. The absence of imaginary frequencies in all cases confirms their dynamic stability (Fig. S2).

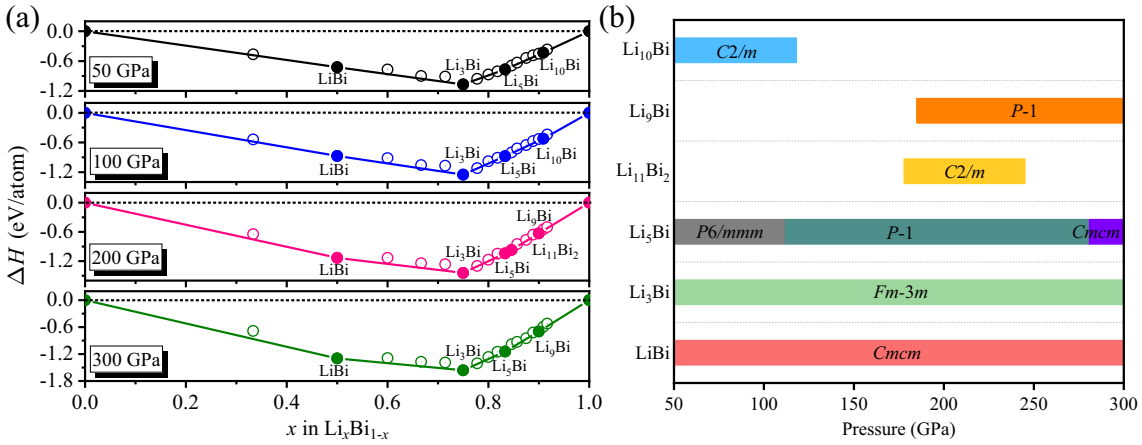


Fig. 1. (a) Convex hulls at 50 GPa, 100 GPa, 200 GPa, and 300 GPa for the lithium-bismuth system. Solid symbols represent thermodynamically stable structures, while hollow symbols represent metastable structures. (b) Pressure-composition phase diagrams from 50 GPa to 300 GPa, where solid symbols indicate enthalpies of formation that lie on the convex hull.

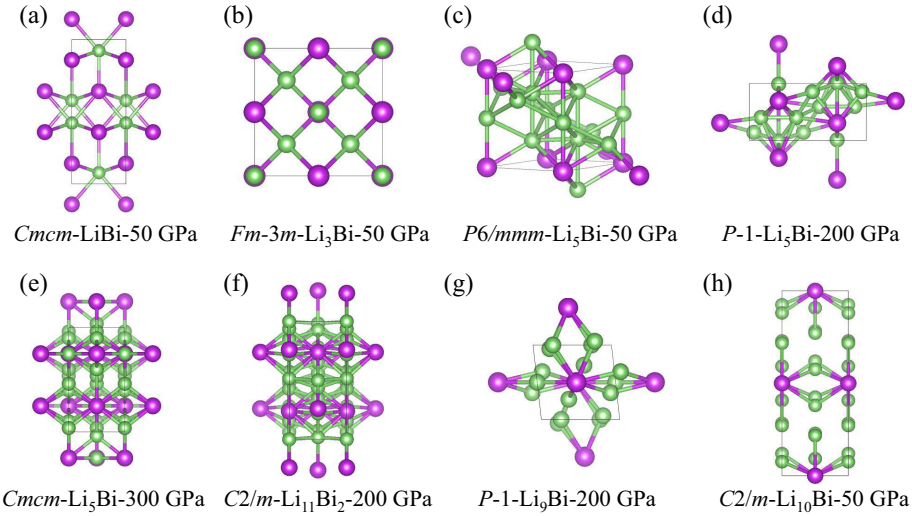


Fig. 2. Crystal structures of stable Li-rich Li_xBi_y compounds. (a) *Cmcm* LiBi at 50 GPa. (b) *Fm*-3*m* Li_3Bi at 50 GPa. (c) *P6/mmm* Li_5Bi at 50 GPa. (d) *P*-1 Li_5Bi at 200 GPa. (e) *Cmcm* Li_5Bi at 300 GPa. (f) *C*2/*m* $Li_{11}Bi_2$ at 50 GPa. (g) *P*-1 Li_9Bi at 200 GPa. (h) *C*2/*m* $Li_{10}Bi$ at 50 GPa.

4. Electronic properties

Each Li atom typically donates one electron, acting as an electron donor, while each Bi atom can accept up to three electrons, functioning as an electron acceptor. As expected, the *Fm*-3*m* phase of Li_3Bi exhibits semiconducting behavior (Fig. S3). Consequently, Li_xBi_y compounds with a Li-to-Bi ratio greater than 3 are more favorable for the formation of electron-rich compounds, characterized by excess electrons beyond those required for simple ionic bonding. The high matching between $3Li^+$ and Bi^{3-} ions leads to the formation of strong ionic bonds between Li and Bi, which is not conducive to closing the energy band gap. In the present study, we, therefore, focus on electron-rich Li_xBi_y phases with $x/y > 3$, specifically Li_5Bi, $Li_{11}Bi_2$, Li_9Bi, and $Li_{10}Bi$. To elucidate the bonding characteristics and electronic nature of these phases, we calculated the electron localization functions (ELF) at representative pressures.[41] As illustrated in Fig. 3, all thermodynamically stable Li–Bi compounds exhibit electron depletion around Li atoms and electron accumulation around Bi atoms, indicative of significant charge transfer from Li to Bi. This behavior is consistent with the ionic bonding nature arising from the large electronegativity difference between Li (0.98) and Bi (2.02).

Intriguingly, in compounds with $x/y > 3$, localized electrons appear in the interstitial regions of the crystal lattice, forming interstitial electrons — a hallmark of electride

behavior.[42] These interstitial electrons exhibit distinct spatial distributions depending on the compound. Notably, in the *C*2/*m* phase of $Li_{10}Bi$, the interstitial electrons form a one-dimensional, zigzag-shaped network. Such a configuration suggests strong directional connectivity, which is particularly favorable for superconductivity in electride-like systems. Electronic structure calculations reveal that Li_5Bi, $Li_{11}Bi_2$, and $Li_{10}Bi$ display clear metallic behavior, while the *P*-1 phase of Li_9Bi shows marginal metallicity (see Fig. S3). Among them, the *C*2/*m* $Li_{10}Bi$ phase is of particular interest, as it features a high concentration of ISQs with robust spatial connectivity characteristics that make it a promising candidate for superconductivity in electron-rich compounds.

We further investigated the electronic properties of the $Li_{10}Bi$ electride compound. As illustrated in Fig. 4(a), the electronic band structure reveals metallic characteristics, as evidenced by two energy bands (band I and II) crossing the Fermi level (E_f). Notably, flat bands primarily contributed by Li and ISQs are observed near E_f along the *M* and Γ–*Z* directions. In contrast, pronounced band dispersions appear in other high-symmetry directions, indicating strong interatomic interactions throughout the crystal lattice. Figure 4(b) shows the Fermi surface (FS) sheets of the I and II bands, where the Fermi velocity is shown using a color scale, with red and blue representing the highest and zero Fermi velocities, respectively.[43] The FS sheet of the I band has a lower Fermi velocity near the *M* point, which is conducive to the formation of strong EPC. The PDOS reveals that states near the Fermi level are predominantly composed of Li-p, Bi-d, and ISQs contributions, forming a Van Hove singularity that enhances the material's electronic conductivity (Fig. 4(c)). Moreover, substantial orbital hybridization among Li, Bi, and ISQs is observed below E_f, indicating that the bonding interactions among these components play a critical role in stabilizing the $Li_{10}Bi$ compound. Given its notable metallicity, we further investigated the intrinsic superconducting properties of $Li_{10}Bi$ at 50 GPa. EPC calculations estimate a T_c of 6.3 K, with an EPC parameter $\lambda = 0.56$ and a Coulomb pseudopotential $\mu^* = 0.1$, indicating that $Li_{10}Bi$ is a promising one-dimensional electride superconductor.

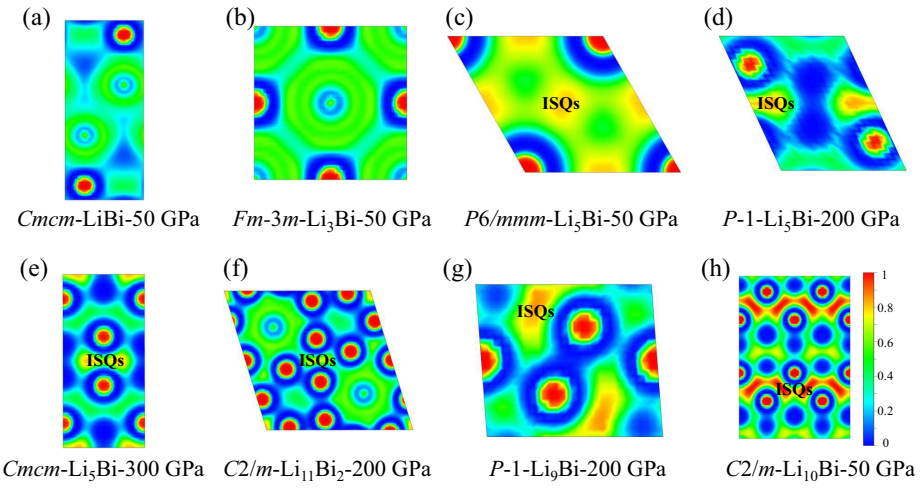


Fig. 3. ELF maps of stable Li-rich Li_xBi_y compounds. (a) *Cmcm* LiBi at 50 GPa in the (100) plane. (b) *Fm*-3*m* Li_3Bi at 50 GPa in the (001) plane. (c) *P6/mmm* Li_5Bi at 50 GPa in the (001) plane. (d) *P*-1 Li_5Bi at 200 GPa in the (001) plane. (e) *Cmcm* Li_5Bi at 300 GPa in the (001) plane. (f) *C*2/*m* $Li_{11}Bi_2$ at 50 GPa in the (010) plane. (g) *P*-1 Li_9Bi at 200 GPa in the (010) plane. (h) *C*2/*m* $Li_{10}Bi$ at 50 GPa in the (001) plane.

5. Superconductivity properties

To elucidate the superconducting mechanism, we calculated the phonon dispersion relations, projected phonon density of states (PHDOS), and Eliashberg spectral function $\alpha^2F(\omega)$ at 50 GPa. The absence of imaginary phonon frequencies confirms the dynamic stability of $Li_{10}Bi$ under this pressure. In addition, significantly softened phonon modes are observed near the high-symmetry *M* and Γ–*Z* directions in the low-frequency region, which are primarily attributed to the lattice vibrations of Li and Bi atoms, as shown in Fig. 4(d). The PHDOS analysis reveals that phonon modes span two frequency regimes: (i) Low-frequency modes (< 110 cm^{-1}), primarily arising from Bi atom vibrations, contribute $\sim 18\%$ to the total EPC strength λ; (ii) High-frequency optical phonons (> 110 cm^{-1}), associated mainly with Li atom vibrations, account for the remaining $\sim 82\%$ of λ (Fig. 4(e)). This suggests that the dominant electron–phonon interaction in $Li_{10}Bi$ arises from the coupling between the electronic states (Li-p, Bi-d, and ISQs) near E_f and the high-frequency Li-derived phonon modes.

Subsequently, we examined the superconducting behavior of $Li_{10}Bi$ under decreasing pressure to assess the pressure dependence of T_c (Fig. 4(f)). Remarkably, $Li_{10}Bi$ remains dynamically stable even at ambient pressure, with an estimated T_c of 0.33 K. The evolution of T_c with pressure exhibits a dome-shaped trend, reaching a maximum of 9.9 K at 35 GPa. Further analysis attributes this variation in supercon-

ductivity primarily to changes in the EPC strength λ under pressure. Analyzing the pressure dependence of λ and the log-mean phonon frequency ($\omega_{\log}$), it is evident that the pressure-induced increase in T_c of $Li_{10}Bi$ is dominated by the increase in λ (0.83 at 35 GPa), whereas $\omega_{\log}$ exhibits an opposite trend, indicating that it has little effect on the T_c evolution of $Li_{10}Bi$.

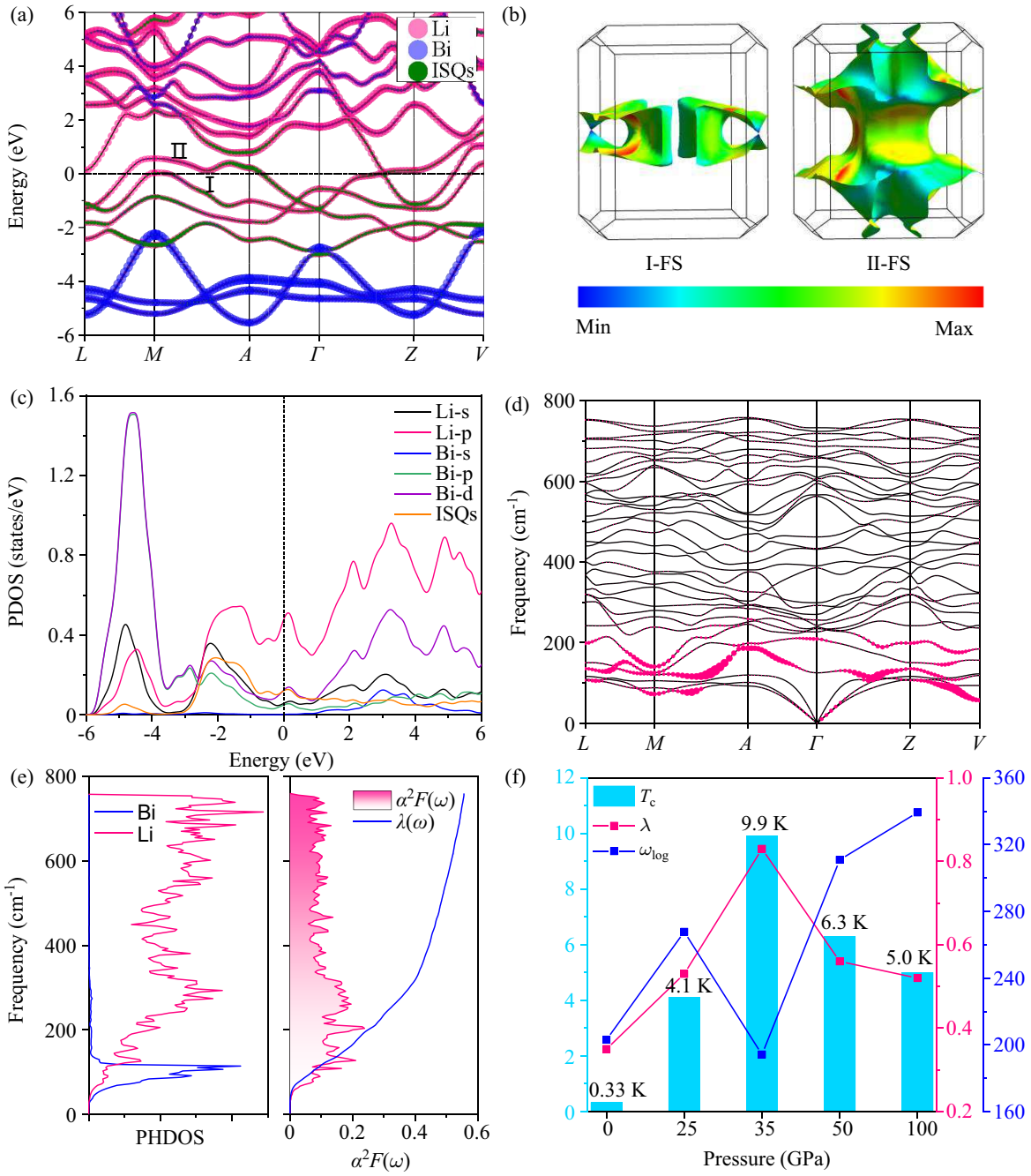


Fig. 4. (a) Electronic band structure of $C2/m$ $Li_{10}Bi$ at 50 GPa. (b) Fermi surfaces corresponding to the two bands crossing the Fermi energy (E_f), colored according to the Fermi velocity. (c) PDOS of $C2/m$ $Li_{10}Bi$ at 50 GPa, showing contributions from Li-p, Bi-d, and ISQs. (d) Calculated phonon dispersion curves of $C2/m$ $Li_{10}Bi$ at 50 GPa. The area of each circle is proportional to the electron–phonon coupling strength λ. (e) PHDOS, Eliashberg spectral function $\alpha^2F(\omega)$, and frequency-dependent electron–phonon coupling parameters $\lambda(\omega)$ of $C2/m$ $Li_{10}Bi$ at 50 GPa. (f) Pressure-dependent λ, $\omega_{\log}$, and T_c of $C2/m$ $Li_{10}Bi$.

6. $Li_{10}Bi$ as a potential lithium battery electrolyte

Recent advances have revealed that certain electronic compounds can enter superionic states, where ions — rather than electrons — become the dominant charge carriers.[44–46] Unlike superconductivity, which arises from the collective motion of delocalized electrons at cryogenic temperatures, superionicity originates from rapid ion migration through lattice vacancies or interstitial channels under thermal excitation. Such materials are of great interest for solid-state lithium batteries, as they can combine structural robustness with high ionic conductivity.[47]

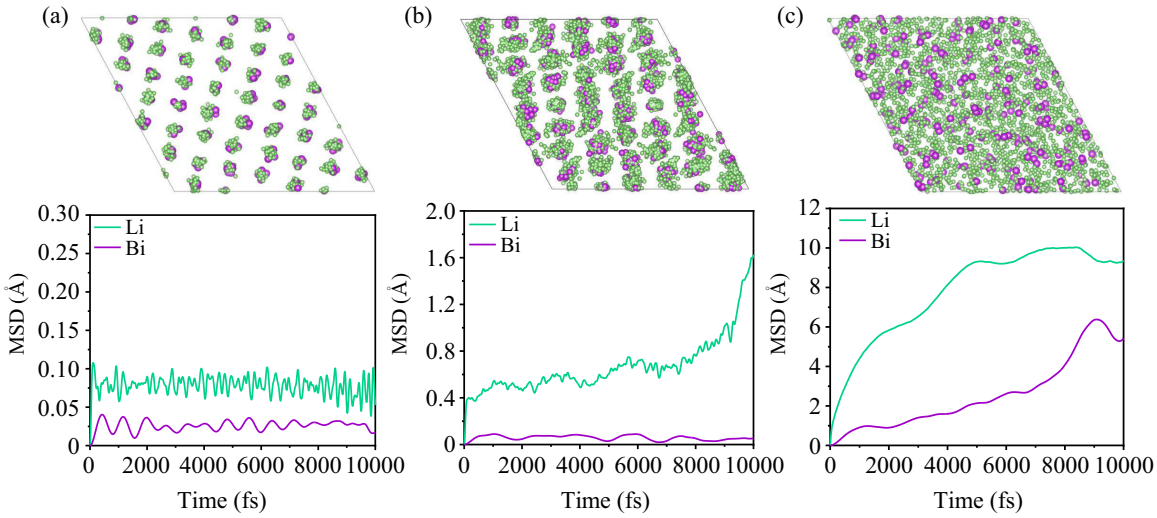


Fig. 5. Evolution of the MSDs of Li and Bi atoms in the *C*2/*m* $Li_{10}Bi$ structure at 0 GPa, shown at three representative temperatures: (a) 300 K, (b) 700 K, and (c) 1500 K.

To investigate the ionic transport behavior of $Li_{10}Bi$, AIMD simulations were performed under ambient pressure to assess its temperature-dependent stability and conductivity (Fig. 5). The results confirm that $Li_{10}Bi$ remains dynamically and structurally stable, suggesting that it may act as a lithium-ion conductor once thermally activated.

At 300 K, both Li and Bi atoms exhibit small vibrational amplitudes confined to their equilibrium positions, with mean-square displacements (MSDs) fluctuating around a constant value, and the calculated diffusion coefficient is zero ($D_{Li} = D_{Bi} = 0$). This indicates a rigid crystalline phase without long-range ionic migration. When the temperature rises to 700 K, the MSDs of Bi atoms remain nearly constant — showing that the heavy Bi atoms are essentially fixed at their potential minima — while Li atoms display a steady, linear increase in MSDs with time. This decoupling of motion is a distinctive feature of superionic conductors, where a stable sublattice supports the fast diffusion of light ions. In $Li_{10}Bi$, the immobile Bi framework provides mechanical and electrochemical stability, while Li^+ ions migrate through interstitial channels, a behavior highly desirable for lithium-battery electrolytes.

The calculated diffusion coefficient for Li^+ at 700 K is $D_{Li} = 6.8 \times 10^{-7}$ $cm^2 \cdot s^{-1}$, corresponding to an estimated ionic conductivity $\sigma_{Li} = 5.9 \times 10^{-1}$ $S \cdot cm^{-1}$ ($\sigma = \frac{nq^2D}{k_BT}$, where the diffusion coefficient D was obtained from the slope of the MSD curve (units: $cm^2 \cdot s^{-1}$), $q = +e$ is the Li^+ charge, and n is the Li^+ number density (cm^{-3})) from the Nernst–Einstein relation. This conductivity is remarkably high — comparable to or exceeding those of molten lithium salts and established high-temperature superionic materials such as Li_3PS_4 ($\sigma \approx 10^{-3}$ $S \cdot cm^{-1}$ at 450 K), β-Li_3N ($\sigma \approx 10^{-4}$ $S \cdot cm^{-1}$ at 300 K), and $Li_{10}GeP_2S_{12}$ ($\sigma \approx 1.2 \times 10^{-2}$ $S \cdot cm^{-1}$ at 298 K).[47–49] These results confirm that $Li_{10}Bi$ exhibits exceptionally fast Li^+ transport once thermally activated. At 1500 K, both Li and Bi atoms exhibit long-range diffusion with linearly increasing MSDs, indicating full lattice melting. The diffusivities reach $D_{Li} = 1.28 \times 10^{-5}$ $cm^2 \cdot s^{-1}$ and $D_{Bi} = 6.64 \times 10^{-6}$ $cm^2 \cdot s^{-1}$, corresponding to $\sigma = 7.45 \times 10^{-2}$ $S \cdot cm^{-1}$.

The sharp increase in Li^+ mobility between 300 K and 700 K signifies a superionic phase transition driven by lattice softening and enhanced Li kinetic energy. The coexistence of an immobile Bi framework and a highly mobile Li sublattice parallels the mechanism of advanced solid electrolytes such as garnet-type $Li_7La_3Zr_2O_{12}$ and sulfide-type $Li_{10}GeP_2S_{12}$, where a rigid host lattice enables Li^+ migration through interconnected pathways.[47,50–52] Although the activation temperature for Li^+ diffusion in $Li_{10}Bi$ ($\sim$ 700 K) exceeds typical battery operating ranges ($<$ 400 K), the underlying physics — a stable heavy-atom framework coupled with light-ion dynamics through interstitial channels — suggests strong potential for designing Bi-based lithium conductors. Through compositional or structural tuning, similar Li-sublattice mobility might be realized at lower temperatures, offering a new design paradigm that bridges electride superconductivity and solid-state lithium-ion transport within a single material system.

7. Conclusion

In this work, we systematically investigated the structural, electronic, and superconducting properties of lithium-rich Li–Bi compounds under high pressure. By combining global structure search with first-principles calculations, we identified several thermodynamically stable electronic compounds, among which $Li_{10}Bi$ exhibits remarkable features, including one-dimensional interstitial electrons, metallicity, and moderate-pressure superconductivity. Notably, $Li_{10}Bi$ reaches a maximum T_c of 9.9 K at 35 GPa, primarily driven by strong EPC involving Li atoms.

$Li_{10}Bi$ is stable at ambient conditions. AIMD simulations

reveal a transition to a superionic state above 700 K, characterized by fast Li^+ diffusion ($D_{Li} = 6.8 \times 10^{-7}$ $cm^2 \cdot s^{-1}$) within an immobile Bi framework. These findings position $Li_{10}Bi$ as a dual-functional quantum material, which has both superconducting electrons and diffusive ions. The coexistence of a rigid heavy-atom lattice and a mobile Li sublattice provides a natural link between electride superconductors and solid-state electrolytes. This insight not only broadens the understanding of electride physics but also introduces a new material-design strategy: engineering interstitial electronic topologies that promote both strong EPC and low-energy ionic transport.

Acknowledgments

Project supported by the National Natural Science Foundation of China (Grant No. U24A2079) and the National Supercomputing Center in Zhengzhou. X. Y. acknowledges the Leverhulme Trust for an Early Career Fellowship (Grant No. ECF-2022-194). This work also made use of the ARCHER2 UK National Supercomputing Service via project e883 and through the UK's HEC Materials Chemistry Consortium, which is funded by the EPSRC (Grant Nos. EP/L000202 and EP/R029431).

References

[1] Wang Y, Jiang K, Ying J, Wu T, Cheng J, Hu J and Chen X 2025 *Natl. Sci. Rev.* **12** nwaf373
[2] Ersoz T T, Mohamed A E-M A and Attallah M M 2025 *Mater. Res. Bull.* **189** 113448
[3] Li Y, Song S, Kim H, Nomoto K, Kim H, Sun X, Hori S, Suzuki K, Matsui N, Hirayama M, Mizoguchi T, Saito T, Kamiyama T and Kanno R 2023 *Science* **381** 50
[4] Bachman J C, Muy S, Grimaud A, Chang H H, Pour N, Lux S F, Paschos O, Maglia F, Lupart S, Lamp P, Giordano L and Shao-Horn Y 2016 *Chem. Rev.* **116** 140
[5] Yu J, Yong X, Lu S and Tse J S 2025 *Chin. J. Chem.* **43** 3699
[6] Wang Q, Zhang S, Li H, Wang H, Liu G, Ma J, Xu H, Liu H and Ma Y 2023 *J. Mater. Chem. A* **11** 21345
[7] Wei J, Zhong T, Sun J, Liu H, Zhu L and Zhang S 2025 *Phys. Rev. B* **111** 184508
[8] Wan B, Zhang J, Wu L and Gou H 2019 *Chin. Phys. B* **28** 106201
[9] Racioppi S and Zurek E 2025 *Annu. Rev. Mater. Res.* **55** 421
[10] Dye J L 2009 *Acc. Chem. Res.* **42** 1564
[11] Zhang X and Yang G 2020 *J. Phys. Chem. Lett.* **11** 3841
[12] Hosono H and Kitano M 2021 *Chem. Rev.* **121** 3121
[13] Zhang X, An T and Yang G 2025 *Comput. Mater. Today* **5** 100020
[14] Tu Z, Sun P, Jia D, Gou H, Liu K and Lei H 2025 *Chin. Phys. Lett.* **42** 027302
[15] Zhao Z, Zhang S, Yu T, Xu H, Bergara A and Yang G 2019 *Phys. Rev. Lett.* **122** 097002
[16] Zhang X, Yao Y, Ding S, Bergara A, Li F, Liu Y, Zhou X F and Yang G 2023 *Phys. Rev. B* **107** L100501
[17] Wang X, Wang Y, Wang J, Pan S, Lu Q, Wang H T, Xing D and Sun J 2022 *Phys. Rev. Lett.* **129** 246403
[18] Han S, Bergara A, Zhang X, Ding S, Li F and Yang G 2025 *Supercond. Sci. Technol.* **15** 100187
[19] Frost M, Kim J B, McBride E E, Peterson J R, Smith J S, Sun P and Glenzer S H 2019 *Phys. Rev. Lett.* **123** 065701
[20] Schaeffer A M J, Talmadge W B, Temple S R and Deemyad S 2012 *Phys. Rev. Lett.* **109** 185702
[21] Struzhkin V V, Eremets M I, Gan W, Mao H K and Hemley R J 2002 *Science* **298** 1213
[22] Chen J H, Iwasaki H and Kikegawa T 1997 *J. Phys. Chem. Solids* **58** 247
[23] Häussermann U, Söderberg K and Norrestam R 2002 *J. Am. Chem. Soc.* **124** 15359
[24] Aoki K, Fujiwara S and Kusakabe M 1982 *J. Phys. Soc. Jpn.* **51** 3826
[25] Yu J, Yong X, Liu H and Lu S 2024 *Phys. Rev. B* **110** 224507
[26] Li Z, Jiang X, Lu G, Deng T, Wang R, Wei J, Zheng W, Yang Z, Tang D, Zhao Q, Hu X, Xu C and Zhou X 2023 *Chem. Eng. J.* **465** 142895
[27] Wang Y, Lv J, Zhu L and Ma Y 2012 *Comput. Phys. Commun.* **183** 2063
[28] Wang Y, Lv J, Zhu L and Ma Y 2010 *Phys. Rev. B* **82** 094116
[29] Kresse G and Furthmüller J 1996 *Phys. Rev. B* **54** 11169
[30] Perdew J P, Burke K and Ernzerhof M 1996 *Phys. Rev. Lett.* **77** 3865
[31] Monkhorst H J and Pack J D 1976 *Phys. Rev. B* **13** 5188
[32] Togo A, Chaput L, Tadano T and Tanaka I 2023 *J. Phys.: Condens. Matter* **35** 353001
[33] Giannozzi P, Baroni S, Bonini N, *et al.* 2009 *J. Phys.: Condens. Matter* **21** 395502
[34] Allen P B and Dynes R C 1975 *Phys. Rev. B* **12** 905
[35] McMillan W L 1968 *Phys. Rev.* **167** 331
[36] Shuichi N 1991 *Prog. Theor. Phys. Suppl.* **103** 1
[37] Hoover W G 1985 *Phys. Rev. A* **31** 1695
[38] Martyna G J, Klein M L and Tuckerman M 1992 *J. Chem. Phys.* **97** 2635
[39] Nosé S 1984 *J. Chem. Phys.* **81** 511
[40] Zhou P, Ni Y, Wang J, Han Y, Li Y, Lu Q, Zhang Z, Wang X and Sun J 2025 *Phys. Rev. B* **111** 134109
[41] Becke A D and Edgecombe K E 1990 *J. Chem. Phys.* **92** 5397
[42] Miao M S and Hoffmann R 2015 *J. Am. Chem. Soc.* **137** 3631
[43] Kawamura M 2019 *Comput. Phys. Commun.* **239** 197
[44] Wang Q, Cui W, Xu W, Gao K, Hao J, Shi J, Liu H and Li Y 2024 *Phys. Rev. B* **110** 134114
[45] Wang X, Tang W, Sun X W, Liu Z J, Cao B, Yang M, Sun Y, Cui T, Li L and Tian F 2024 *ACS Mater. Lett.* **6** 3697
[46] Xu W, Wang Q, Zeng Q, Li X, Shi J, Hao J, Cui W and Li Y 2025 *Comput. Mater. Today* **5** 100017
[47] Kamaya N, Homma K, Yamakawa Y, Hirayama M, Kanno R, Yonemura M, Kamiyama T, Kato Y, Hama S, Kawamoto K and Mitsui A 2011 *Nat. Mater.* **10** 682
[48] Lapp T, Skaarup S and Hooper A 1983 *Solid State Ionics* **11** 97
[49] de Klerk N J J, van der Maas E and Wagemaker M 2018 *ACS Appl. Energy Mater.* **1** 3230
[50] Meier K, Laino T and Curioni A 2014 *J. Phys. Chem. C* **118** 6668
[51] Murugan R, Thangadurai V and Weppner W 2007 *Angew. Chem. Int. Ed.* **46** 7778
[52] Mo Y, Ong S P and Ceder G 2012 *Chem. Mater.* **24** 15